LUND UNIVERSITY

Studies of time-resolved harmonic generation in intense laser fields in xenon

Faldon, M. E; Hutchinson, M. H. R; Marangos, J. P; Muffett, J. E; Smith, R. A; Tisch, J. W. G; Wahlström, Claes-Göran

Published in:
Journal of the Optical Society of America B: Optical Physics

DOI:
10.1364/JOSAB.9.002094

1992

Link to publication

Citation for published version (APA):
Faldon, M. E., Hutchinson, M. H. R., Marangos, J. P., Muffett, J. E., Smith, R. A., Tisch, J. W. G., & Wahlström, C.-G. (1992). Studies of time-resolved harmonic generation in intense laser fields in xenon. *Journal of the Optical Society of America B: Optical Physics*, *9*(11), 2094-2099. https://doi.org/10.1364/JOSAB.9.002094

Total number of authors:
7

General rights
Unless other specific re-use rights are stated the following general rights apply:
Copyright and moral rights for the publications made accessible in the public portal are retained by the authors and/or other copyright owners and it is a condition of accessing publications that users recognise and abide by the legal requirements associated with these rights.
• Users may download and print one copy of any publication from the public portal for the purpose of private study or research.
• You may not further distribute the material or use it for any profit-making activity or commercial gain
• You may freely distribute the URL identifying the publication in the public portal

Read more about Creative commons licenses: https://creativecommons.org/licenses/

Take down policy
If you believe that this document breaches copyright please contact us providing details, and we will remove access to the work immediately and investigate your claim.

LUND UNIVERSITY

PO Box 117
221 00 Lund
+46 46-222 00 00

Download date: 17. Dec. 2025

Studies of time-resolved harmonic generation in intense laser fields in xenon

M. E. Faldon, M. H. R. Hutchinson, J. P. Marangos, J. E. Muffett, R. A. Smith, J. W. G. Tisch, and C. G. Wahlstrom*

Blackett Laboratory, Imperial College, London SW7 2BZ, UK

Received July 30, 1991; revised manuscript received May 5, 1992

We report preliminary experimental and computational studies of the temporal evolution of the harmonics, generated in xenon, by 50-ps pulses from a Nd:YLF laser, amplified in Nd:glass amplifiers, and focused to produce intensities in the range 10^{13}–5×10^{13} W cm^{-2}. Measurements were made of the temporal profiles of the seventh- and ninth-order harmonics using a specially modified VUV streak camera with better than 7-ps temporal resolution. These results were compared with predictions of a numerical model that included the effects of neutral atom depletion and photoelectron dispersion in the calculation of the harmonic output as a function of time.

INTRODUCTION

The generation of harmonics of high-intensity laser radiation in rare gases has been shown to be an effective mechanism for the production of coherent XUV radiation.[1] The shortest harmonic wavelengths have been produced by high-intensity KrF lasers (249 nm), with which orders up to 25 (9.96 nm) have been produced.[2] However, with the development of high-brightness neodymium lasers, harmonic orders as high as 53 (19.9 nm) have been produced with laser intensities in the range 10^{13} to 5×10^{14} W cm^{-2}.[3]

At these high intensities, additional nonlinear processes in the medium [e.g., multiphoton ionization (MPI) and an intensity-dependent refractive index] can influence strongly the efficiency of harmonic generation. In particular, MPI of the rare gas decreases the number of neutral species being driven. This process would be expected to cause saturation of harmonic generation. In principle, this may be offset by contributions from the singly and, subsequently, multiply ionized species. The nonlinear susceptibilities of the ions are unknown at present but are expected to be substantially smaller than that of the neutral species. A significant effect also arises from the additional optical dispersion of the photoelectrons, the density of which is both space and time dependent, and this modifies the phase mismatch of the fundamental and harmonic radiation in a complicated fashion. Both of these phenomena lead to a change in the temporal and spatial characteristics of the fundamental beam and its harmonics from that predicted for lower laser intensities.

In this paper we report the first results in an experimental study of the temporal evolution of the seventh and ninth harmonics of a Nd:YLF laser (1.053 μm) produced in xenon. A numerical model of the nonlinear process of harmonic generation is described briefly. This takes into account the time- and space-dependent ionization of the medium and dispersion of the photoelectrons. It illustrates how these effects influence the temporal profile of the harmonics under different experimental conditions. Contributions from ionized species are ignored. Other intensity- and time-dependent phenomena, such as intensity-dependent resonances, a nonlinear refractive index, and modifications to the spatial and temporal profiles of the laser pulse, are not included in the model at this stage.

EXPERIMENTAL DETAILS

We employed a mode-locked Nd:YLF oscillator that produced 5-nJ pulses of duration 40–50 ps in a 75-MHz pulse train. Individual pulses from the train were amplified in a regenerative amplifier, followed by two further amplifiers, to an energy of up to 40 mJ. The high amplification factor (10^7) modified somewhat the temporal profile of the amplified pulses. Owing to fluctuations in the oscillator/amplifier, there was some shot-to-shot variation in these temporal shapes. To account for this in the investigations, we monitored the temporal shape of each pulse using an IR-sensitive streak camera (Hadland Imacon 500) with a 5-ps temporal resolution. This was essential, bearing in mind the high-order nonlinearity of the processes being studied. The laser-pulse energies were monitored with the use of a fast photodiode positioned to detect laser light transmitted by a beam-turning mirror. This detector was cross calibrated against a calorimeter and was used to determine the total pulse energy of each shot.

The beam of diameter 10 mm (at the e^{-2} intensity points) was telescoped down to 3.7 mm and focused with a 200-mm focal length best-form lens into a pulsed jet of xenon, positioned close to the entrance plane of a 1-m normal-incidence VUV monochromator. The choice of the focusing optics was determined by several factors. First, efficient generation of the harmonics imposes the conflicting requirements of a large value of the confocal parameter (b) of the beam[4] and an intensity in the interaction region that is high enough to permit the generation of harmonics of sufficient intensity for time-resolved detection. Second, a large confocal beam parameter accompanies a relatively small beam size on the diffraction grating, where excessive power density causes permanent damage, but which is nonetheless required to maximize the temporal resolution (see below). The beam divergence

0740-3224/92/112094-06$05.00 © 1992 Optical Society of America

was approximately diffraction limited. We measured the diameter at the e^{-2} position of the focal spot to be 70 μm, using photographic film located at the focal point with the beam adequately attenuated to avoid film saturation. This corresponded to a confocal parameter of $b = 7$ mm. A maximum intensity of the focused pulse of 5×10^{13} W cm^{-2} could be achieved.

The pulsed gas jet (Lasertechnics LPV) provided a sufficiently dense gas volume for efficient harmonic generation. However, the pulsed operation ensured that the background pressure did not exceed 10^{-4} Torr at anytime and was compatible with the operation of the VUV streak camera. A measurement of the absolute atomic density distribution in the jet was made with a differential interference technique[5] and showed values in the range 10^{17}–10^{18} cm^{-3} with an approximately Lorentzian density distribution with a FWHM of 1 mm.

Dispersion of the harmonic spectrum was performed with a 1-m normal-incidence McPherson VUV monochromator fitted with a 1200-line/mm grating with a MgF_2/Al coating. This enabled us to examine the temporal structure of a single harmonic order while introducing only a small temporal spread due to the grating dispersion. One can estimate an upper limit to this spread by taking the diameter of the harmonic beam at the grating as equal to that of the fundamental (18.5 mm). The temporal spread is given for the first diffraction order by $N\lambda/c$ (where N is the total number of rulings illuminated). For the seventh harmonic (150 nm), this spread is thus 11 ps. The divergences of the seventh and higher harmonics are expected to be significantly smaller than that of the fundamental,[6] by a factor of $1/\sqrt{q}$ for Gaussian beams assuming no saturation effects, leading to proportionately smaller temporal spreads (4 ps for the seventh harmonic). Since the grating had low efficiency below 110 nm, the present preliminary study was restricted to the seventh and ninth harmonics.

As we described above, the time dependences of the fundamental and harmonic pulses were measured with two electro-optic streak cameras operated simultaneously, which provided direct shot-to-shot comparison of their temporal profiles. The VUV streak camera was positioned with the photocathode close to the exit plane of the monochromator, which was used without an entrance slit. A CsI photocathode was specially developed and provided a sensitivity approximately 100 times that of conventional CsI systems for wavelengths near 150 nm, corresponding to the wavelength of the seventh harmonic. This was achieved by careful optimization of both the CsI structure and the supporting substrate. We determined the temporal resolution of the camera using pulses of subpicosecond duration (measured by autocorrelation) with a wavelength of 249 nm. These were generated in a mode-locked dye laser (497 nm) and, after amplification and frequency doubling, were further amplified in a KrF system. The measured temporal resolution for the VUV streak camera with an entrance slit of width 350 μm (the narrowest slit that still permitted a sufficiently large signal to be recorded) was 7 ps. During the harmonic time-resolution experiments the streak camera was operated without a slit, but the image size on the photocathode of the harmonic radiation did not exceed 100 μm and thus was less than the 350-μm slit aperture used in calibration. The calibration then sets an upper limit of 7 ps on the actual temporal resolution during the experiments. The resolution of the IR streak camera was 5 ps.

Images from both streak cameras were enhanced with image intensifiers and recorded on photographic film (HP5). The film was developed in a carefully controlled manner to ensure that well-established film curves could be used in determining accurately the relative intensity variations with time. A microdensitometer, with scanning slits set to match closely the streak camera resolutions, was used to trace the photographically recorded data. This effectively smoothed out the effects of film/intensifier graininess that might have distorted the traces on a shorter distance scale than that equivalent to the streak camera temporal resolution.

NUMERICAL MODEL

The numerical model describes the generation of the electric field of the qth harmonic at frequency $q\omega$ in a nonlinear medium that is undergoing MPI by a focused Gaussian fundamental beam of radiation of frequency ω. The electric field $\mathbf{E}(\mathbf{r}', t)$ at the position $\mathbf{r}'$ outside the nonlinear medium, generated by a polarization $\mathbf{P}(\mathbf{r}, t)$ at $\mathbf{r}$, is given by[7,8]

$$\mathbf{E}_q(\mathbf{r}', t) = \nabla \wedge \nabla \wedge \int \frac{\mathbf{P}_q(r)\exp[-i\omega_q(t - l/c)]}{R} \mathrm{d}V, \quad (1)$$

where R is the distance between the volume element $\mathrm{d}V$ and the point of observation and $\mathbf{P}_q$ is the component of the induced nonlinear polarization oscillating at frequency $\omega_q (= q\omega)$. The parameter l is the optical path length between the points $\mathbf{r}$ and the observation point $\mathbf{r}'$.

The relationship between the nonlinear polarization and the driving field, the single-atom response, has been widely discussed.[9] In particular, the origin of the experimentally observed plateau in harmonic intensity as a function of harmonic order has attracted considerable interest. Single-atom effects, such as the dynamic Stark shift of bound-state energy levels in the neutral atom, are expected to contribute to the intensity dependence as well as to the temporal profiles of the harmonics. This is true in particular for the higher harmonics, in which Stark shifting of Rydberg states may introduce intensity-dependent, and thereby space- and time-dependent, intermediate resonances. In these cases significant deviations from the expressions given by lowest-order perturbation theory are expected. However, experimental data[4] suggest that at these intensities deviations from lowest-order perturbation theory are relatively small for the lower harmonics and that the harmonic intensity scales with laser intensity approximately as I^q. This is in agreement with the predictions of lowest-order perturbation theory. In this study we have therefore concentrated on the effects of photoionization of the medium and use lowest-order perturbation theory to express the single-atom response. The relationship between the nonlinear polarization $P_q(r, t)$ and the driving electric field $E_1(r, t)$ is

$$\mathbf{P}_q(\mathbf{r}, t) = (2^{q-1})^{-1}\left[\sum_i N_i(\mathbf{r}, t)\chi_i^{(q)}\right]\mathbf{E}_1^q(\mathbf{r}, t), \quad (2)$$

where $\chi_i^{(q)}$ is the qth-order nonlinear susceptibility of the

atomic (or ionic) species i and $N_i(\mathbf{r},t)$ is the spatially and temporally dependent atomic (or ionic) number density.

For simplification, it is assumed that the spatial dependence of the laser radiation is described by a Gaussian beam propagating in the positive z direction. However, as we will illustrate below, the predicted temporal profiles of the harmonics are highly dependent on the radial profile of the focused laser beam. The temporal profile of the driving field could be chosen either to have a smooth model shape or to match exactly the shape of individual harmonic pulses measured in the experiment.

If photoionization and intensity-dependent contributions to the refractive index were to be ignored, the phase mismatch between the polarization field and the generated harmonic wave, given by $\Delta k_q = k_q = qk_1 = (n_q - n_1)q\omega/c$, could be treated as being independent of $\mathbf{r}$ and t (assuming that the laser beam diameter is much smaller than the width of the nonlinear medium). The harmonic signal may then be obtained analytically by integration over the focal region and the detection plane,[8] giving

$$I_q = g(q)k_q[\chi^{(q)}]^2 N_0{}^2 I_1{}^q |F_{(q)}|^2, \tag{3}$$

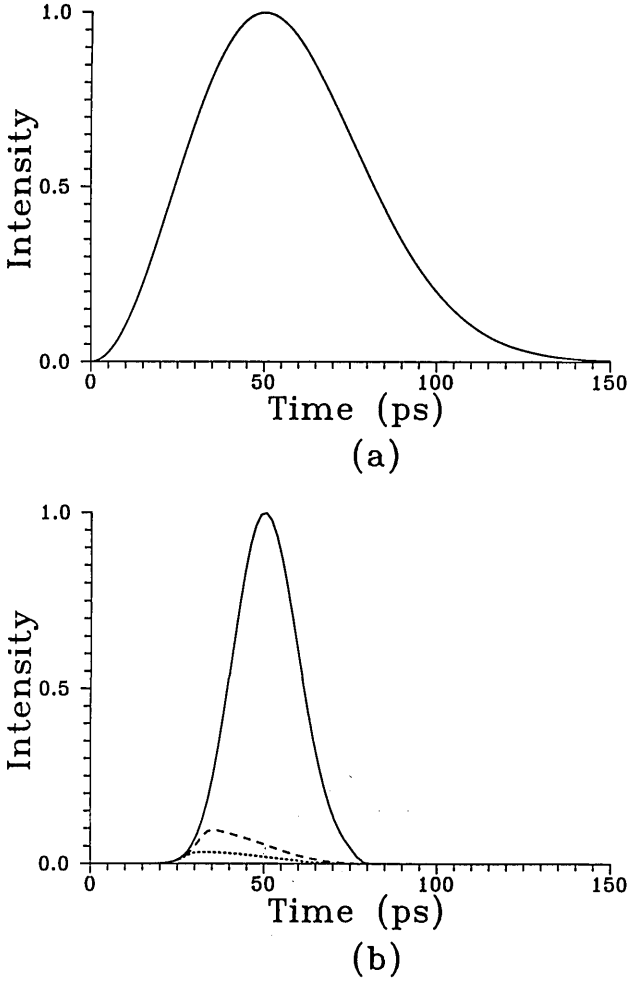

Fig. 1. (a) Temporal profile of model laser pulse (modified Gaussian). (b) Calculated temporal profiles of the seventh harmonic (arbitrary units) at laser intensity 2.5×10^{13} W cm^{-2} with no saturation (solid curve), with neutral atom depletion (no contribution from ions) but no photoelectron dispersion (dashed curve), and with both neutral atom depletion and photoelectron dispersion (dotted curve).

where $g(q)$ is a function only of q, the harmonic order, and N_0 is the peak number density of the gas. $F_{(q)}$ is the phase-matching integral

$$F_{(q)} = \frac{2}{b}\int_{-\infty}^{\infty} \frac{S(z)}{(1+i\epsilon)^{q-1}} \exp\left[-i\int_{-\infty}^{z} \Delta k(z'')\mathrm{d}z''\right]\mathrm{d}z, \tag{4}$$

where $\epsilon = 2(z - z_0)/b$, b is the confocal parameter of the focused beam, and $S(z)$ is the normalized gas density profile.

Photoionization affects the harmonic intensity principally in two ways. First, the density of neutral atoms is reduced, and the densities of ions of different ionization stages are increased. The nonlinear response of the different ionization stages is not known precisely, and we are therefore restricted to making rather crude assumptions about the role played by the ions. Second, the free electrons liberated in the ionization process affect the dispersive properties of the nonlinear medium.

If a neutral gas with a pressure of 15 Torr is fully (but singly) ionized, the density of free electrons will be approximately 5×10^{17} cm^{-3}. In this case the plasma frequency ω_p is much less than the optical frequencies, and the phase mismatch in the electron gas,

$$\Delta k_q = (n_q - n_1)q\omega/c = \omega_p{}^2(q^2 - 1)/2q\omega c, \tag{5}$$

is positive and increases with harmonic order. This is dominated by the free-electron refractive index at the laser frequency (ω). If we use theoretical *ab initio* values for the dynamic polarizabilities in the weak-field limit from Ref. 10, an estimate of, e.g., Δk_7, with a density corresponding to the experimental condition ($p = 15$ Torr) and a laser wavelength of 1.053 μm, gives $\Delta k_7 = 3.3$ cm^{-1} in neutral xenon and, for a free-electron gas with the same number density, $\Delta k_7 = 110$ cm^{-1}. Clearly the phase mismatch due to the free electrons completely dominates the mismatch due to the dispersion in the neutral gas.[4,10] Positive contributions of the above magnitude to the phase mismatch reduce the value of the phase-matching integral for the seventh and ninth harmonics, and consequently the harmonic intensities, by several orders of magnitude. However, in studies of the temporal profiles of the harmonic intensities, it is the intermediate region, where the nonlinear medium is neither neutral nor fully (singly) ionized, that must be considered. As the laser intensity increases during the rise time of the laser pulse, the harmonic intensity initially increases as $[I(t)]^q$ according to Eq. (3). However, as the laser intensity increases further, the rate of photoionization also increases, saturating first the central region of the focus, where the intensity is highest, and then spreading outward, both radially and along the z axis. As this photoionization develops in time and space, the phase matching is affected in increasingly larger zones of the interaction region. The time development of the harmonic intensity can therefore not be expected to follow an I^q law. Any attempt to predict the time development must include this complex space and time dependence of the phase-matching condition. In addition, the time dependence of the harmonic intensity will also be related to the rate of depletion of the atoms and the relative susceptibilities of the ions and the neutral atoms.

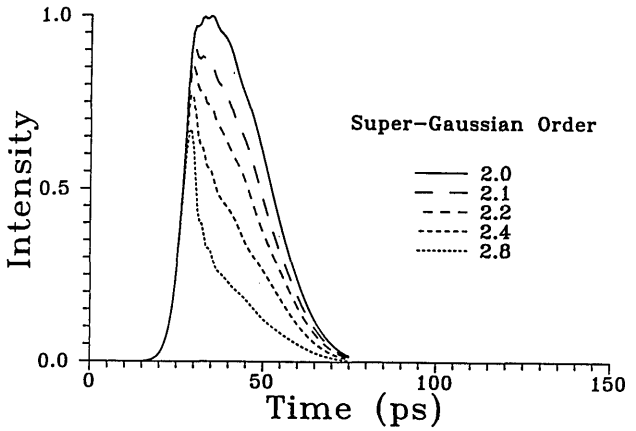

Fig. 2. Dependence of the seventh-harmonic temporal profile [with the same laser temporal profile as for Fig. 1(a)] on the spatial profile of the laser beam. The conditions are as for Fig. 1(b) (dotted curve) but with super-Gaussians of differing order. Note the decrease in both duration and intensity as the super-Gaussian order increases.

In our model we have included both the time- and space-dependent phase matching and depletion of the neutral atoms that are discussed above and calculated numerically the temporal profile for the harmonic intensity. First, for each grid point in time, the density of neutral atoms, electrons, and ions of different ionization stages (determined from lowest-order perturbation theory) and the local phase mismatch are calculated at every grid point (r, z) in space. Second, the amplitude and the phase for the partial waves, originating in different concentric cylinders, are calculated through numerical integration in the z direction for each value in the r grid. Finally, the total field at the point of observation on the z axis far from the interaction region is obtained through integration over r.

Some of the results obtained by the model described above are illustrated in Fig. 1. The normalized harmonic intensity for $q = 7$ is plotted versus time together with the normalized laser-pulse intensity, which is given by $I(t) = I_0(t/\tau)^2 \exp[-(t/\tau)^2]$, for $t \geq 0$. The radial density profile is given by a lowest-order Gaussian beam profile. The solid curve is obtained for an intensity of 2.5×10^{13} W cm^{-2}, but the presence of photoelectrons is ignored and the ions Xe^+ and Xe^{2+} are assumed to have the same susceptibilities as that of neutral xenon. This is equivalent to ignoring the effect of both neutral atom depletion and photoelectron dispersion. The dashed curve shows the effect of neglecting both ionic contributions to the susceptibility and photoelectron dispersion, thus accounting for neutral atom depletion. The dotted curve shows the effect of neglecting the ionic susceptibility but including

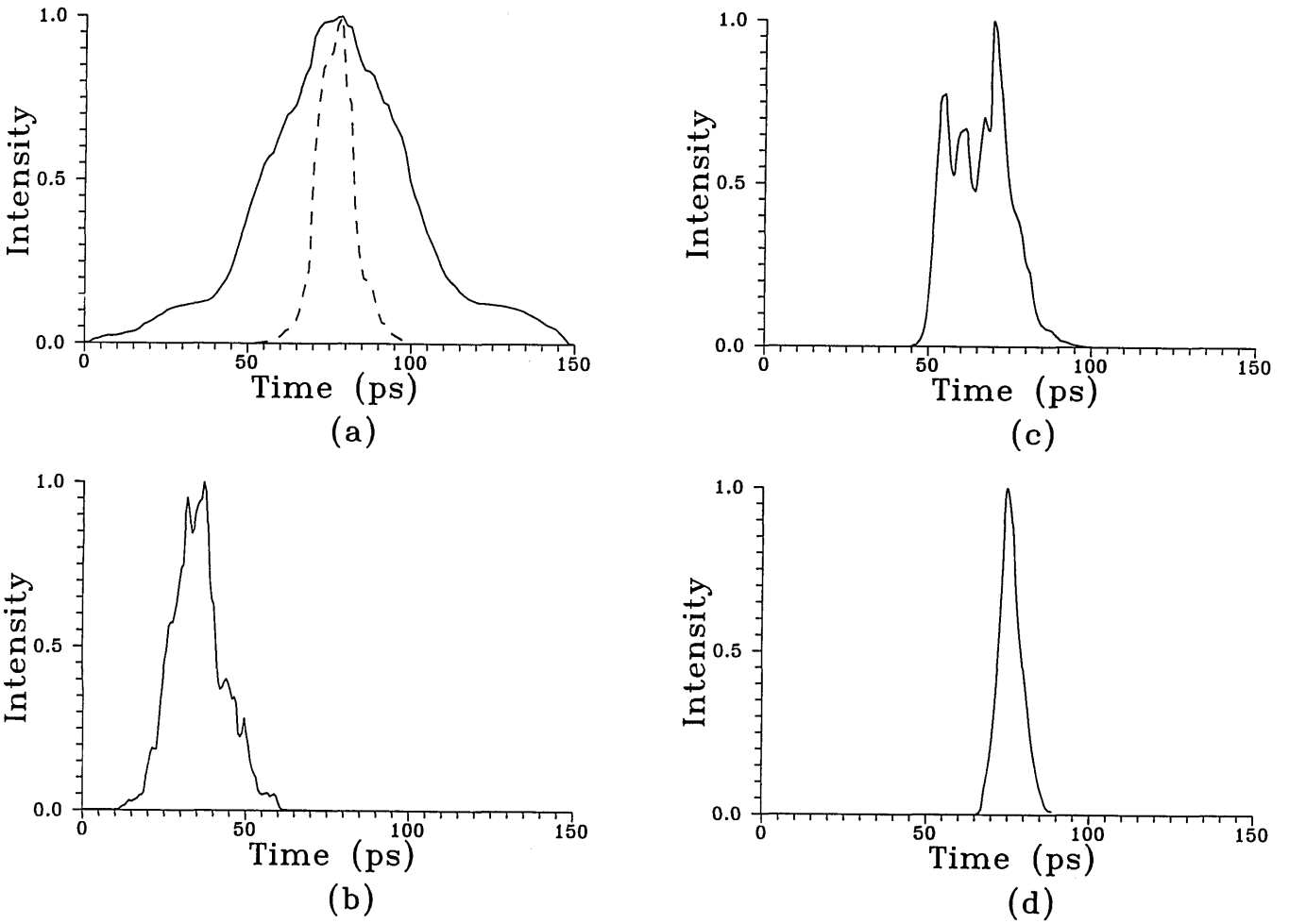

Fig. 3. (a) Measured temporal profile of the incident laser pulse (solid curve) and the expected ninth harmonic in the absence of saturation (dashed curve). (b) Measured temporal profile of the ninth harmonic. (c) Calculated temporal profile of the ninth harmonic. (d) Measured temporal profile of the subpicosecond UV pulse from the VUV streak camera.

the photoelectron dispersion. The inclusion of photoelectron dispersion results in a substantial reduction in the harmonic intensity, the peak is shifted in time, the pulse width (T_{FWHM}) is increased, and the profile is asymmetric.

In Fig. 2 the effect on the temporal profile of varying the radial beam profile of the driving laser is illustrated by a few examples. The calculations include the effects of both neutral atom depletion and photoelectron dispersion, but with different orders of a super-Gaussian spatial profile, i.e., $I(r) = I_0 \exp[-2(r/r_0)^n]$. Thus the dotted curve in Fig. 1(b) corresponds to the solid curve in Fig. 2 for a super-Gaussian of order $n = 2$. This illustrates the sensitive dependence of the harmonic temporal profiles on the spatial profile of the focused laser beam.

RESULTS

A large number of data shots were recorded, essentially under identical conditions (notwithstanding fluctuations in the temporal profile and the intensity of the laser). Data were recorded for both the seventh and ninth harmonics. The eleventh harmonic was also observed and time resolved, but the intensities were too low to permit quantitative analysis (a consequence of the grating efficiency). The dynamic range of the VUV streak camera was 1:20. With shot-to-shot fluctuations in laser intensities and the high nonlinearity of the process, many shots either gave intensities too low to be detected or saturated the streak camera. Therefore it was necessary to eliminate these shots from the data set. Also, streaks of the IR laser that showed sharp intensity spikes and complex temporal structure were rejected. Examples of the ninth- and seventh-harmonic data are shown below in Figs. 3 and 4, respectively.

We employed the numerical model to investigate the role of MPI and electron dispersion, using the measured parameters for a given laser shot. The measured laser temporal profile was used, along with the measured laser-pulse energy and the spatial characteristics of the focused pulse, to determine the instantaneous intensity at each spatial position in the focus. A Gaussian beam profile was assumed and taken to have the same width as the measured beam waist (70-μm diameter). This assumption was dictated by the absence of a sufficiently detailed measured spatial profile, and thus only the diameter of the beam could be determined with confidence from the data. A gas density distribution with a FWHM of 1 mm and a peak density of 5×10^{17} cm^{-3} is used in the calculation. The computed profiles are relatively insensitive to the gas jet density but are sensitive to the precise details of both the spatial and temporal laser intensity profiles.

Figure 3 compares the time dependence of the fundamental [Fig. 3(a)] and the ninth harmonic [Fig. 3(b)] for a typical pulse with a peak intensity of 3.4×10^{13} W cm^{-2}. The intensities are normalized and, as we described above, noise induced by the photographic film used in the streak camera that was below the temporal resolution has been smoothed. Also shown in Fig. 3(a) is the result (normalized to the same scale) of raising the laser intensity profile to the ninth power (I^9), which is the expected form of the ninth-harmonic profile in the absence of any saturation effects. The measured temporal profile of the 249-nm subpicosecond pulse is also shown [Fig. 3(d)] and indicates the 7-ps temporal resolution of the VUV streak camera. In the calculated profile [Fig. 3(c)] it is assumed that the contribution of ions to the harmonic intensity is negligible, but depletion of the neutral atoms and photoelectron dispersion are both included. Figure 4 shows a similar set of results for the seventh harmonic for an incident pulse intensity of 3.2×10^{13} W cm^{-2}. The time axes

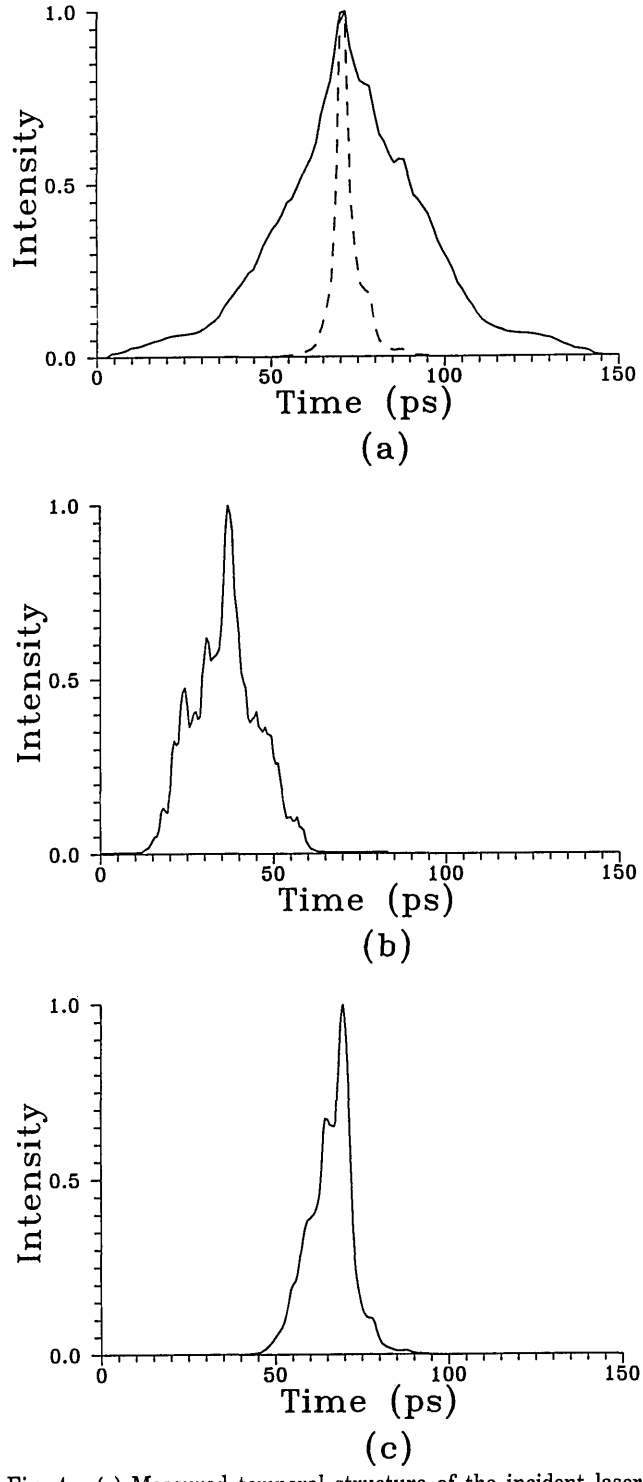

Fig. 4. (a) Measured temporal structure of the incident laser pulse (solid curve) and the expected seventh harmonic in the absence of saturation (dashed curve). (b) Measured temporal profile of the seventh harmonic. (c) Calculated temporal profile of the seventh harmonic.

of the temporal profiles of the fundamental and harmonic pulses are absolute, but their relative synchronization has yet to be determined.

A notable feature of these data is the significantly shorter duration of the harmonic pulses compared with that of the fundamental pulses. A reduction in duration of approximately a factor of 3 can be seen for both the seventh and ninth harmonics. This pulse shortening is a consequence of the high-order nonlinearity of the process. In the absence of any saturation the temporal profiles would be expected to be given by the FWHM of the normalized curves plotted for I^q [Figs. 3(a) and 4(a)]. The measured results are longer than these in both cases, markedly so for the seventh harmonic. We believe that this result is the first experimental determination of the temporal structure of high harmonics obtained at high laser intensities.

A qualitative comparison between the calculated results and the measured data reveals similarities. In both sets of data (Figs. 3 and 4) the temporal durations of measured and calculated profiles are longer than that found from the I^q curves. For the ninth-harmonic profiles, agreement is apparent for the overall form of the rising and falling edges. The structure near the peak of the measured and calculated ninth-harmonic profiles does not show detailed agreement. The 7-ps resolution of the VUV camera restricts the detection of the temporal structure of the measured harmonic. Also, the 5-ps resolution of the IR camera limits detailed knowledge of the temporal pulse, and errors are magnified in the calculation of the harmonic profile owing to the high-order nonlinearity of the process. In addition, the calculated result was found to be highly sensitive to the spatial profile of the laser beam used in the calculation (see Fig. 2) above. This may have a significant effect on the agreement between measured and calculated results, since detailed information about the actual focused laser beam profile was absent.

For the seventh harmonic the shapes of the rising edge of the calculated and measured profiles are qualitatively similar, although the falling edge drops off significantly more quickly for the calculated result. This degree of disagreement is not surprising given the relative simplicity of the model and the sensitivity of the calculation to the spatial and temporal profiles of the laser pulse.

In addition to radiation at the harmonics, significant background emission was observed at frequencies other than those of the odd harmonics. Studies of the time evolution of this background indicate two components. A slow component turns on and decays over a period of 5–10 ns and is suggestive of a recombination mechanism. However, a prompt component is also observed that is coincident in time with the laser pulse; its origin is as yet unclear.

CONCLUSION

We have demonstrated the feasibility of measurements of the temporal profiles of harmonics, which provides an additional tool in understanding the role of neutral atom depletion and photoelectron dispersion in the dynamics of harmonic generation at high laser intensities. The results obtained so far indicate two main features. First, an obvious temporal shortening of the harmonics compared with the laser pulse is apparent in all the cases. Second, there appears to be significant deviation for the experimental results from the temporal form predicted from a straightforward I^q scaling. A simplified numerical model, which includes multiphoton ionization effects (neutral atom depletion and photoelectron dispersion), provides, in significant respects, a better match to the experimental data.

Further research on both improving the experiments and developing a more complete numerical model is now under way. In particular, better characterization of the laser beam spatial profile, as well as improvement of the temporal resolution of the streak cameras, is important in establishing a stronger agreement between measurement and calculation. A careful study of the dependence of the temporal profile on parameters such as intensity, beam profile, and focusing geometry can now be contemplated.

ACKNOWLEDGMENTS

We are grateful to Luan Shuwen for his assistance in the operation of the laser system employed in this study. This research was carried out in the Blackett Laboratory Laser Consortium with financial support by the Science and Engineering Research Council (SERC) and the Ministry of Defence. The loan of an IR-sensitive streak camera by the Rutherford Appleton Laboratory is gratefully acknowledged. J. P. Marangos is supported by a SERC Advanced Fellowship.

*Present address, Department of Physics, Lund Institute of Technology, Box 118, S-22100 Lund, Sweden.

REFERENCES

1. For a review, see A. L'Huillier, L. A. Lompre, G. Mainfray, and C. Manus, "High-order harmonic generation in rare gases," Adv. At. Mol. Opt. Phys. (to be published).
2. N. Sarukura, K. Hata, T. Adechi, R. Nodomi, M. Watanabe, and S. Watanabe, Phys. Rev. A **43,** 1669 (1991).
3. A. L'Huillier, L. A. Lompre, G. Mainfray, and C. Manus, in *Proceedings of the Fifth International Conference on Multiphoton Physics* (Commisariat a l'Energie Atomique, Paris, 1990), pp. 1–355.
4. L. A. Lompre, A. L'Huillier, M. Ferray, P. Monot, G. Mainfray, and C. Manus, J. Opt. Soc. Am. B **7,** 754 (1990).
5. G. W. Faris and H. M. Hertz, Appl. Opt. **28,** 4662 (1989).
6. G. Hilber, D. J. Brink, A. Lago, and R. Wallenstein, Phys. Rev. A **38,** 6231 (1988).
7. N. Bloembergen and P. S. Pershan, Phys. Rev. Lett. **128,** 606 (1962).
8. A. Lago, G. Hilber, and R. Wallenstein, Phys. Rev. A **36,** 3827 (1987).
9. K. Kulander and A. L'Huillier, eds., feature on high-order processes in atoms, J. Opt. Soc. Am. B **7,** 401 (1990); K. Burnett and M. H. R. Hutchinson, eds., feature on multiphoton physics, J. Mod. Opt. **36,** 811 (1989).
10. A. L'Huillier, X. F. Li, and L. A. Lompre, J. Opt. Soc. Am. B **7,** 527 (1990).